Available online at www.sciencedirect.com
ScienceDirect
Physics Letters A 365 (2007) 421–428
PHYSICS LETTERS A
www.elsevier.com/locate/pla

# The solar activity cycle is weakly synchronized with the solar inertial motion

Milan Paluš [a,*], Jürgen Kurths [b], Udo Schwarz [b], Norbert Seehafer [b], Dagmar Novotná [c], Ivanka Charvátová [d]

[a] *Institute of Computer Science, Academy of Sciences of the Czech Republic, Pod vodárenskou věží 2, 182 07 Prague 8, Czech Republic*
[b] *Department of Physics, Potsdam University, Am Neuen Palais 10, D-14469 Potsdam, Germany*
[c] *Institute of Atmospheric Physics, Academy of Sciences of the Czech Republic, Boční II/1401, 141 31 Prague 4, Czech Republic*
[d] *Institute of Geophysics, Academy of Sciences of the Czech Republic, Boční II/1401, 141 31 Prague 4, Czech Republic*

Received 3 December 2004; received in revised form 29 January 2007; accepted 30 January 2007

Available online 3 February 2007

Communicated by A.P. Fordy

**Abstract**

We study possible interrelations between the 300-year record of the yearly sunspot numbers and the solar inertial motion (SIM) using the recently developed technique of synchronization analysis. Phase synchronization of the sunspot cycle and the SIM is found and statistically confirmed in three epochs (1734–1790, 1855–1875 and 1907–1960) of the whole period 1700–2000. These results give quantitative support to the hypothesis that there is a weak interaction between the solar activity and the SIM.


*PACS:* 05.45.Tp; 05.45.Xt; 95.75.Wx; 96.60.Qc

*Keywords:* Sunspot cycle; Solar inertial motion; Phase synchronization; Hypothesis testing; Surrogate data

## 1. Introduction

Regularities and irregularities in the solar activity cycle [1] are among the most intriguing and poorly understood aspects of the Sun. Dynamo theory [2–4], describing complex magnetohydrodynamic plasma motions inside the Sun, has resulted in many models which reproduce basic features of solar activity [5–7]. However, the nature of the solar cycle is far from being understood. Attempts have been made to identify signatures of low-dimensional chaos in the sunspot data [8–10], however, the used algorithms have been found unreliable when applied to noisy and possibly non-stationary experimental data.

The hypothesis that the gravitational forces exerted upon the Sun by the giant planets in the solar system can influence the solar activity cycle has been discussed for decades [11–14], however, until now possible connections were only described in qualitative or indirect ways. The recently developed concept of phase synchronization in complex systems [15–19] provides a highly efficient method for the detection and quantitative assessment of a weak interaction between two processes represented by possibly nonlinear, noisy, non-stationary and relatively short time series. In this Letter we present such a synchronization analysis of the sunspot numbers and the solar inertial motion. We find with high statistical significance that there are decadal epochs where these two oscillatory phenomena are probably phase synchronized. This result provides the first quantitative evidence that the motion of the giant planets has some influence on the dynamics of the solar cycle.

## 2. Solar inertial motion and sunspots: The data

In reaction to movements of the planets in the solar system, the Sun moves around the barycenter (the center of mass) of the solar system, as already noted by Newton in his *Principia*: "... since that center of gravity (center of mass of the solar system) is continually at rest, the Sun, according to the various positions of the planets, must continually move every way, but

* Corresponding author.
*E-mail address:* mp@cs.cas.cz (M. Paluš).

0375-9601/$ – see front matter 
doi:10.1016/j.physleta.2007.01.039

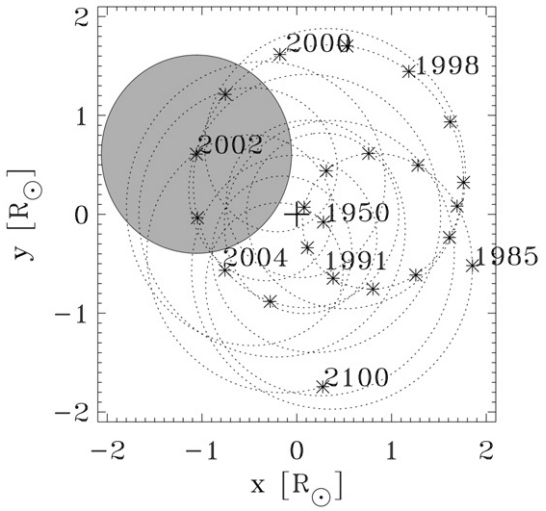


Fig. 1. Trajectory of the SIM in the period 1949–2100 A.D. The barycenter of the solar system is located at + and the positions of the Sun are marked by ∗. The orbital rotation of the Sun is anti-clockwise. The shadowed circle shows the solar disk in January 2002, when the barycenter was clearly outside the Sun.

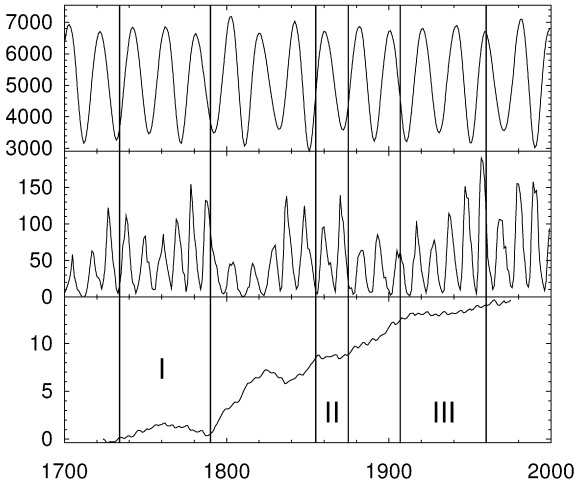


Fig. 2. Top panel: Radius of curvature of the trajectory of the solar inertial motion (SIM), calculated according to (1) from the Sun's coordinates relative to the solar system barycenter with the invariable plane as the reference $x$–$y$ plane, for the period 1700–2000. Middle panel: Yearly sunspot numbers for the period 1700–2000. Bottom panel: Phase difference between the instantaneous phases of the radius of curvature of the SIM trajectory and the (band-pass filtered) sunspot cycle. The solid vertical lines are the borders of the epochs in which the sunspot cycle is phase synchronized with the SIM. These epochs are 1734–1790 (marked as I), 1855–1875 (marked as II) and 1907–1960 (marked as III).

will never recede far from that center." [20]. This movement, called the *solar inertial motion* (SIM hereafter), is confined to a region with a diameter of 4.34 solar radii, that is 0.02 AU (astronomical units) or $3 \times 10^6$ km. For comparison, the eccentricity of the Earth's orbit is $5 \times 10^6$ km. The SIM mainly reflects movements of the two largest planets—Jupiter (orbit period of about 11.86 years) and Saturn (about 29.45 years), which account for 93% of the total planetary mass, however, other planets influence the SIM, too. As a result, the trajectory of the Sun around the barycenter (which is often outside the Sun) is a complicated composition of loops and arcs (Fig. 1). Similar motions of other stars yield a part of the oscillatory Doppler shift of their spectral lines, which is also an important signature of extrasolar planets [21].

The SIM, i.e., the temporal evolution of the coordinates $x, y, z$ of the Sun relative to the barycenter has been calculated using the procedure of Shirley [22]. The solar motion is largely determined by the positioning of the giant planets Jupiter, Saturn, Uranus, and Neptune. Thus the core of the solar motion program used here is an algorithm for the heliocentric ecliptic of date planetary positions published by Van Flandern and Pulkkinen [23], listing nearly 300 periodic terms for longitude, latitude, and distance from the Sun of the 4 giant planets. Clemence [24] gives formulae for calculating the position of the solar system barycenter. The planetary positions are corrected for precession and obliquity, to refer to the ecliptic of 1950.0. Planetary mass values are those employed in the Jet Propulsion Laboratory development ephemeris DE-102 [25].

Here we use the coordinates of the center of the Sun relative to the solar system barycenter with the solar system invariable plane as the reference $x$–$y$ plane. Two rotations convert the 1950 ecliptic frame positions into invariable plane coordinates. The new positive $x$ direction corresponds to the node of the invariable plane on the 1950 ecliptic, at longitude $107°16'38.96''$. The inclination correction is $1°39'16.47''$. Having computed the coordinates $x, y, z$, any function descriptive of the Sun's motion can be found. Here we analyze the radius of curvature, $\rho$, of the Sun's orbit, computed from the components of the SIM velocity and acceleration, i.e., from the first-order and second-order temporal derivatives of the Sun's coordinates $x, y, z$:

$$\rho = v^3 / \sqrt{(\dot{y}\ddot{z} - \dot{z}\ddot{y})^2 + (\dot{z}\ddot{x} - \dot{x}\ddot{z})^2 + (\dot{x}\ddot{y} - \dot{y}\ddot{x})^2}, \tag{1}$$

where the dots mean temporal derivatives and the velocity $v$ is defined as

$$v = \sqrt{\dot{x}^2 + \dot{y}^2 + \dot{z}^2}. \tag{2}$$

Using Shirley's algorithm [22], the coordinates $x, y, z$ were generated with daily sampling in order to obtain smooth estimates of their first-order and second-order derivatives. Then the values of the curvature radius $\rho$ as given by (1) were computed and averaged in order to obtain the series $\{\rho(t)\}$ (where $t = 1, 2, \ldots$ stands for time) with yearly sampling (Fig. 2, top panel), which can be analyzed together with the series $\{S(t)\}$ of the yearly sunspot numbers from the period 1700–2000 (Fig. 2, middle panel) [26]. It should be mentioned that $\rho$ oscillates with a period of about 20 years. Therefore, we have to test for a possible 2 : 1 synchronization of SIM and solar activity [see Eq. (6) below]. Prior to further processing, the sunspot series has been filtered by a simple moving average (MA) band-pass filter: First, the MA's from a 13-sample (year) window have been subtracted from the data in order to remove slow processes and trends, and then a 3-sample MA smoothing has been used in order to remove high-frequency components and noise.

## 3. Synchronization analysis: The method

Based on the concept of phase synchronization of chaotic oscillators [15,19], a new technique has been developed to ana-

lyze complex, even non-stationary, bivariate data [16–18]. First, we calculate the instantaneous phases $\phi_S(t)$ and $\phi_\rho(t)$ of the sunspot cycle and the SIM's curvature radius, respectively. The instantaneous phase and amplitude of a signal $s(t)$ can be determined by using the analytic signal concept of Gabor [27], recently introduced into the field of nonlinear dynamics within the context of chaotic synchronization [15,16]. The analytic signal $\psi(t)$ is a complex function of time defined as

$$\psi(t) = s(t) + j\hat{s}(t) = A(t)e^{j\phi(t)}, \tag{3}$$

where the function $\hat{s}(t)$ is the Hilbert transform of $s(t)$,

$$\hat{s}(t) = \frac{1}{\pi}\text{P.V.}\int_{-\infty}^{\infty}\frac{s(\tau)}{t-\tau}\,d\tau. \tag{4}$$

(P.V. means that the integral is taken in the sense of the Cauchy principal value.) $A(t)$ is the instantaneous amplitude and the instantaneous phase $\phi(t)$ of the signal $s(t)$ is

$$\phi(t) = \arctan\frac{\hat{s}(t)}{s(t)}. \tag{5}$$

Here we use a discrete version of the Hilbert transform (4) with a finite (25-sample) summation window instead of the infinite integration interval in (4). Having the instantaneous phases $\phi_S(t)$ and $\phi_\rho(t)$ of the sunspot cycle and the SIM's curvature radius, respectively, we define the instantaneous 2 : 1 phase difference

$$\Delta\phi(t) = 2\phi_\rho(t) - \phi_S(t). \tag{6}$$

In the classical case of periodic self-sustained oscillators phase synchronization is defined as phase locking, i.e., the phase difference is constant. In the case of phase-synchronized chaotic or other complex systems fluctuations of phase difference typically occur. Therefore, the criterion for phase synchronization is that the absolute values of $\Delta\phi$ must be bounded [15]. When the instantaneous phases are not represented as cyclic functions in the interval $[0, 2\pi)$ but as monotonously increasing functions on the whole real line, then also the instantaneous phase difference $\Delta\phi(t)$ is defined on the real line and is an unbounded (increasing or decreasing) function of time for asynchronous states of systems, while epochs of phase synchronization appear as plateaus in the $\Delta\phi(t)$ vs. time plots.

## 4. Results and their statistical evaluation

In Fig. 2, bottom panel depicting $\Delta\phi(t)$ (6), one can identify three plateaus in the periods 1734–1790, 1855–1875, and 1907–1960 (marked as I, II and III, respectively). For obtaining quantitative evidence that these periods are epochs in which the sunspot cycle is phase synchronized with the SIM, we use ideas of Stratonovich [28] and consider phase locking in a statistical manner, i.e., as appearance of a peak in the distribution of the cyclic relative phase (phase difference)

$$\Delta\psi = \Delta\phi \bmod 2\pi. \tag{7}$$

We estimate $\Delta\psi$ distributions as histograms with 16 bins on the interval $[0, 2\pi)$. The histograms for the above epochs

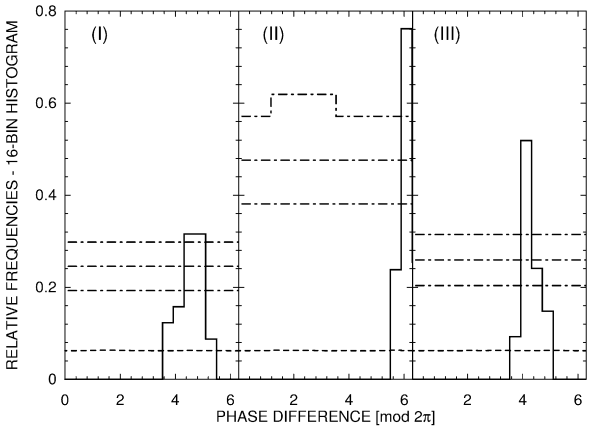


Fig. 3. Histograms of the cyclic relative phases (phase differences) $\Delta\psi$ of the sunspot cycle and the radius of curvature, $\rho$, of the SIM trajectory (thick solid lines) for the epochs 1734–1790 (I), 1855–1875 (II) and 1907–1960 (III). Also shown are the histograms of related surrogate (Barnes model vs. $\rho$) sets: Dashed lines correspond to average histograms and dash-and-dotted lines, from bottom to top, show the 95th, 97.5th and 99th percentiles of the frequency value distributions in each of the 16 histogram bins.

I, II and III (Fig. 3, solid lines) are strongly localized around particular values and are clearly different from a uniform distribution which should be generated by phase differences of non-synchronized systems. Considering, however, the small amounts of samples in the scrutinized epochs, the differences from a uniform $\Delta\psi$ distribution should be statistically evaluated. Employing the concept of surrogate data [10,29,30], we generate 131,000 independent realizations of the Barnes model [31],

$$z_i = \alpha_1 z_{i-1} + \alpha_2 z_{i-2} + a_i - \beta_1 a_{i-1} - \beta_2 a_{i-2}, \tag{8}$$

$$s_i = z_i^2 + \gamma\left(z_i^2 - z_{i-1}^2\right)^2, \tag{9}$$

where $\alpha_1 = 1.90693$, $\alpha_2 = -0.98751$, $\beta_1 = 0.78512$, $\beta_2 = -0.40662$, $\gamma = 0.03$ and $a_i$ are independent, identically distributed Gaussian random variables with zero mean and standard deviation SD = 0.4.

The model (8), (9) effectively mimics main statistical properties of the sunspot cycle, however, by construction is independent of the SIM. It is not used here to model the physics of the solar cycle, but to produce realizations of a process with similar frequency content as the sunspot cycle. These artificial data will be processed in order to assess whether such a process could randomly produce epochs which appear like phase synchronized with the SIM, like those observed using the real sunspot data. Each realization of the Barnes model is processed in the same way as the original sunspot numbers, so we can estimate the ranges of frequency (relative count) values in each histogram bin.

Using 131,000 surrogate realizations yields 131,000 histograms for any of the epochs I, II and III. Each histogram is estimated using the same number of samples as the related histogram of $\Delta\psi$ of the sunspots vs. $\rho$. Then for each histogram for every bin there are 131,000 count values which are sorted, their distribution is constructed and values for the mean and selected percentiles in every bin are evaluated. Here we present

the 95th, 97.5th and 99th percentiles (dash-and-dotted lines in Fig. 3) of the surrogate distribution in each histogram bin for each of the three histograms for the epochs I, II, and III. These percentiles are "significance levels" for rejecting the null hypothesis of a uniform $\Delta\psi$ distribution, i.e., the hypothesis that the sunspot cycle and the SIM are not phase synchronized. In each of the three scrutinized histograms of the sunspot cycle vs. SIM's $\rho$ cyclic relative phases $\Delta\psi$ there are one or two bins whose values are higher than the related 99th percentile of the surrogate distributions (Fig. 3). Thus the null hypothesis that the phases of the sunspot cycle and of the SIM are independent has been rejected with $p < 0.01$, where $p$ is the level of significance.

In addition, we quantify the histograms by using the concept of Shannon entropy,

$$H = -\sum_{i=1}^{16} p_i \log p_i, \tag{10}$$

where $p_i$ is the relative frequency of occurrence of a value of the relative cyclic phase difference $\Delta\psi$ in a particular histogram bin. The Shannon entropy is maximized for a uniform distribution. So we test whether the Shannon entropy for the scrutinized $\Delta\psi$ histograms is significantly smaller than its values obtained from the Barnes surrogate data, which are not synchronized with the SIM. Here we directly estimate the "significance" of the test by counting the percentage of the surrogate data Shannon entropy values which are smaller than or equal to the value obtained from the tested histogram. This "significance" is in fact a probability that such a value (as obtained from the sunspot data vs. SIM) can randomly occur without any phase synchronization (i.e., that similar synchronous epochs can occur by chance in data with frequency content similar to the sunspot data).

Finally, we use a simple trigonometric statistic, also known as the mean resultant length [32]:

$$\gamma^2 = \big\langle \cos\big(\Delta\psi(t)\big)\big\rangle^2 + \big\langle \sin\big(\Delta\psi(t)\big)\big\rangle^2, \tag{11}$$

where $\langle\,\rangle$ means the temporal average. This trigonometric statistic tends to zero for $\Delta\psi$ of asynchronous processes and to one for phase locked systems. Again, the Barnes model is used as the asynchronous null hypothesis and the significance evaluation is equivalent to the case of the Shannon entropy, however, now we evaluate whether $\gamma$ for the sunspots vs. $\rho$ is significantly larger then $\gamma$'s for the surrogates. In all the tests, employing the Shannon entropy and the trigonometric statistic $\gamma$, the phase synchronization of the sunspot cycle with the SIM has been confirmed with high statistical significance (from $p < 0.02$ to $p < 0.003$).

## 5. More statistical testing

The above statistical tests support our claim that the plateaus observed in the phase difference $\Delta\phi(t)$ vs. time plot are probably caused by phase synchronization between the solar inertial motion and the solar activity cycle. The probability of a random occurrence of such plateaus in synchronization analyses of independent oscillatory systems with the same frequency contents is very low. The plateaus in the studied data, however, were selected by a visual inspection, i.e., the segments with the highest potential for the presence of phase synchronization were selected and then tested against segments of the same length at the same temporal positions in surrogate data. This approach, in the following referred to as the "simple testing", can be biased in favour of false detection of phase synchronization, since a segment with a higher potential for synchronous behavior could occur at a different position in time in a surrogate data realization. For a fully correct test we need to evaluate the probability of an occurrence of a synchronous segment (a plateau) anywhere regardless of its temporal position. It is certainly impossible to search visually for plateaus in a large number of surrogate data realizations. Therefore, for each tested epoch of the scrutinized data (the plateaus) we determine—in each realization of the surrogate data—a segment of the same length which minimizes (over the 300-year surrogate data realization) the Shannon entropy of the $\Delta\psi$ distribution.

For the correct application of this "testing with entropy minimization" approach, however, it is important to test all three segments simultaneously, i.e., to search for three disjoint segments minimizing the Shannon entropy of the $\Delta\psi$ distribution estimated from the same number of $\Delta\psi$ samples as the number of samples in the tested epoch. While using the simple testing approach, the simultaneous and the individual testings give the same results, the individual testing with the entropy minimization decreases the significance for either the short epoch II or the epoch I. The segment I is characterized by a slightly wider $\Delta\psi$ histogram and thus by a higher Shannon entropy than the other epochs. It is not clear whether this "weaker" synchrony in the epoch I is an actual phenomenon or just a consequence of a worse quality of the sunspot data from the 18th century. The requirement of the simultaneous occurrence of three segments in each surrogate data realization, as it is observed in the real sunspot data, is strong enough to reject the hypothesis that the plateaus occurred by chance.

Applying this strengthened testing approach for evaluation of the histograms of the cyclic relative phase $\Delta\psi$ (Fig. 4) we can see that the significance levels (percentiles) are at higher positions than in the previous simple test (cf. Fig. 3). This decreases the significance of the results for the epoch I to $p < 0.025$, which is, however, still highly significant. In the epochs II and III there is always one bin whose value is clearly higher than the 99th percentile of the surrogate distribution (Fig. 4). Thus the null hypothesis of uniform $\Delta\psi$ distribution, i.e., the hypothesis that the phases of the sunspot cycle and of the SIM are independent, has been rejected with $p < 0.01$. Applying the test with the Shannon entropy (10) and the trigonometric statistic (11), the phase synchronization of the sunspot cycle with the SIM has been confirmed with statistical significance from $p < 0.03$ to $p < 0.07$.

The phenomenon of phase synchronization could be mimicked by a trivial phase locking if two oscillatory processes have the same constant frequencies (or different constant frequencies in a rational ratio). In order to demonstrate that this is not the case in the present study, in Fig. 5 we present his-

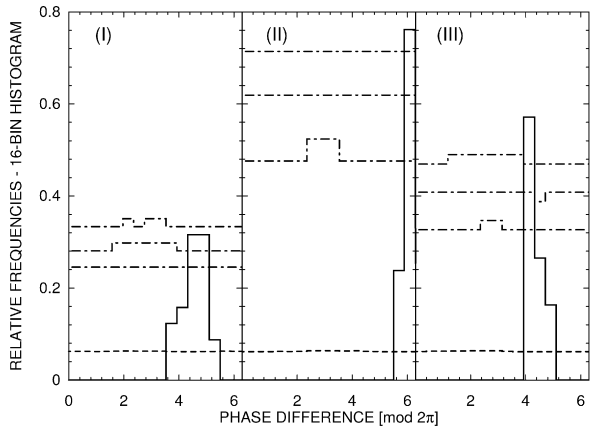


Fig. 4. Histograms of the cyclic relative phases (phase differences) $\Delta\psi$ of the sunspot cycle and the radius of curvature, $\rho$, of the SIM trajectory (thick solid lines) for the epochs 1734–1790 (I), 1855–1875 (II) and 1907–1960 (III) together with histograms of the related surrogate (Barnes model vs. $\rho$) segments which minimize the Shannon entropy of the $\Delta\psi$ distribution. Dashed lines correspond to average histograms and dash-and-dotted lines, from bottom to top, show the 95th, 97.5th and 99th percentiles of the frequency value distributions in each of the 16 histogram bins.

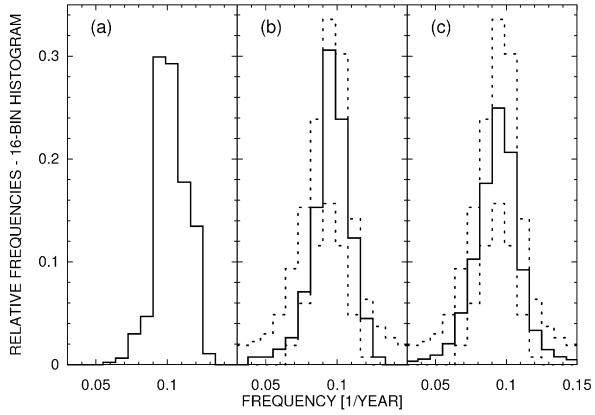


Fig. 5. Histograms of the instantaneous frequencies of (a) the radius of curvature, $\rho$, of the SIM trajectory (the frequency multiplied by two is used), (b) the sunspot cycle (solid line) and (c) the Barnes model—the solid line corresponds the mean histogram of 131,072 300-year realizations. The dashed lines in (b) and (c) show the 5th (lower dashed line) and the 95th (upper dashed line) percentiles of the Barnes model surrogate frequency value distributions in each of the 16 histogram bins.

tograms of instantaneous frequencies $f_\rho$ of the SIM curvature radius $\rho$, (Fig. 5a; the histogram of $2f_\rho$ is plotted) and $f_S$ of the sunspot cycle (Fig. 5b, solid line). Simultaneously, we can assess the adequacy of the Barnes model (8), (9) as surrogate data for the sunspot cycle. The variability of histograms of the instantaneous frequencies obtained from 300-year realizations of the Barnes model is presented by the 5th and the 95th percentiles (dashed lines in Fig. 5b) of the relative count value distributions in each bin of these histograms. The same percentiles together with the mean surrogate histogram (solid line) are presented in Fig. 5c. Both the SIM and the sunspot cycle are narrow-band oscillatory processes, however, their frequencies are variable. The variability of the sunspot cycle frequency does not differ from that of realizations of the Barnes model.

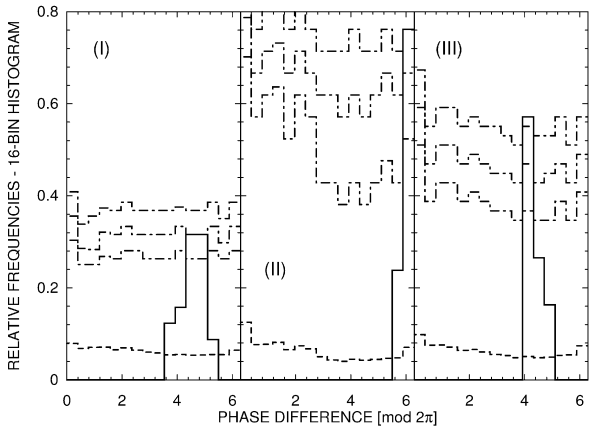


Fig. 6. Histograms of the cyclic relative phases (phase differences) $\Delta\psi$ of the sunspot cycle and the radius of curvature, $\rho$, of the SIM trajectory (thick solid lines) for the epochs 1734–1790 (I), 1855–1875 (II) and 1907–1960 (III) together with histograms for the related surrogate data (sunspot data with randomly permutated cycles vs. $\rho$) segments which minimize the Shannon entropy of the $\Delta\psi$ distribution. Dashed lines correspond to average histograms and dash-and-dotted lines, from bottom to top, show the 95th, 97.5th and 99th percentiles of the frequency value distributions in each of the 16 histogram bins.

Nevertheless, we repeated all the above described tests using the amplitude-adjusted Fourier transform surrogate data [29,30] which almost exactly preserve the spectrum and thus the frequency distribution. The obtained results were fully consistent with those obtained in the above tests with the Barnes model.

According to a referee's recommendation we have repeated the tests with surrogate data constructed from the sunspot data by random permutations of individual cycles. We performed the randomization in the wrapped phase representation—the mixing of individual "saw-teeth" of the phase rising from $-\pi$ to $\pi$ is technically simpler than the mixing of individual cycles of the raw data. Each phase "saw-tooth" contains information about the cycle length (consists of the same number of samples as the original cycle) as well as about the intra-cycle dynamics. Random reordering of the cycles ($-\pi$ to $\pi$ "saw-teeth" in the phase representation) provided a new type of surrogate data used in the same tests as the previously considered realizations of the Barnes model and the AA FFT surrogates. Application of the simple testing approach yielded results fully consistent with those obtained in the testing with the Barnes model surrogate data. Some differences can be observed when these "cycle mixing" surrogates are used in the testing with the entropy minimization approach. The histograms of the sunspot cycle vs. SIM's $\rho$ cyclic relative phases $\Delta\psi$ with the related percentiles (significance levels) for the "cycle mixing" surrogates are presented in Fig. 6. One can see that with the entropy minimization the "cycle mixing" surrogates do not provide enough variability for the percentile values to converge to a single value independent of $\Delta\psi$. Using the highest estimate for the percentiles, however, the $\Delta\psi$ histograms for all three epochs significantly differ from a uniform distribution with $p < 0.05$. (Using the "local" estimates of the percentiles, $p < 0.05$ holds for the epoch I, while $p < 0.01$ holds for the epochs II and III.) The significance of the tests with the Shannon entropy (10) and the trigonometric statistic (11) decreased to values about $p < 0.1$. Using this type

of surrogate data the significance of test results decreases, i.e., the value of $p$ giving the probability of random occurrence of a synchronous segment increases. Not only the truly synchronous segments contribute to the increased $p$ value, but due to a recurrent behavior of the SIM, the sunspot cycles from the epoch I would synchronize with the SIM in the segment III and vice versa, as well as various combinations of these cycles could contribute to the increase of the $p$ value. It is also interesting to note that the phase difference between the SIM and the solar cycle in segments I and III is between 4 and 5 radians, while the preferred phase difference in the "cycle mixing" surrogate data is 0 or $2\pi$ (Fig. 6). Nevertheless, the histograms of the cyclic relative phases $\Delta\psi$ of the sunspot cycle and the radius of curvature, $\rho$, of the SIM trajectory differ from the corresponding $\Delta\psi$ distributions for these surrogate data and $\rho$ on the significance level $p < 0.05$, which supports the claim that in the tested epochs, the SIM and the solar activity are phase synchronized.

## 6. Possible physical mechanisms underlying the synchronization

In this section we briefly discuss possible physical interaction mechanisms of the SIM with the solar activity cycle.

The dynamo for the solar magnetic field is assumed to operate in the convection zone, a spherical shell below the surface of the Sun with a thickness of about 0.3 solar radii, and active regions are believed to result from the emergence of magnetic flux tubes which have broken away from a toroidal field (which is azimuthal with respect to the spin axis of the Sun) in the convection zone and are carried up by magnetic buoyancy. The toroidal field below the surface is generated from a poloidal one (whose field lines lie in planes containing the spin axis) by differential rotation, i.e. velocity shear resulting from the dependence of the spin rate on radius and latitude, while the regeneration of the poloidal field is thought to be accomplished by the alpha effect [2], namely the generation of a mean or large-scale electromotive force by small-scale or turbulent fluid motions that are helical due to the action of Coriolis forces. In some models the toroidal field consists of an ensemble of flux tubes which are stored in a layer close to the bottom of the convection zone and whose rise is initiated by a flux tube instability [33]; in these models the action of Coriolis forces on unstable flux tubes gives rise to an alpha effect [34]. It is common to all models that distortions, changes or modulations of the Sun's own rotation should be reflected in the properties of the activity cycle. Correspondingly, spin–orbit coupling has been suggested as an explanation for correlations between solar activity and the barycentric orbital motion of the Sun [35–37], using as an argument the fact that the orbital angular momentum of the Sun is of the order of 10% of its spin angular momentum and varies by an order of magnitude over a period of $\approx 10$ years. However, no physical model of the solar spin–orbit coupling has been elaborated yet.

Spin–orbit coupling of a celestial body can occur if its mass distribution deviates from spherical symmetry, the degree of asymmetry being measured by the gravitational quadrupole moment of the body. Such deviations from spherical symmetry may be due to permanent deformations, tidal effects or rotational flattening [38]. Since the Sun is in a plasma state, permanent deformations can presumably be excluded. The tidal forces exerted by the planets at the surface of the Sun are $\sim 10^{-12}$ of the solar surface gravity. For comparison, the corresponding ratio for the tidal effect of the Moon on the Earth is $10^{-7}$. Because of the weakness of the tidal forces and also because no convincing evidence for correlations with the activity phenomena or the SIM were found, there seems to be largely agreement now that the planetary tidal influence on solar activity is negligible [12,37,39]. This should also apply to tidal effects on the buoyancy instability of magnetic flux tubes and their rise through the convection zone, since the effective gravitational potential, which determines the behavior of the flux tubes, deviates only by $\sim 10^{-12}$ from the unperturbed potential (though, as simulations for close binary stars show, tidal perturbations $\sim 10^{-3}$ can still have significant effects [40,41]).

Then there remains the solar oblateness $f = (R_{\text{equatorial}} - R_{\text{pole}})/R_{\text{equatorial}} \sim 10^{-5}$ [42] as a possible source of spin–orbit coupling. This oblateness corresponds to a difference of 7 km between the equatorial and polar solar radii, which is at least large compared with the height of the tides raised by the planets ($\lesssim 1$ mm). For comparison, the oblateness of the Earth is $\approx 0.003$ and leads to the precessional motion of the spin axis with its period of 26,000 years, which is even still under discussion as a possible driving mechanism for the geodynamo [43]. The orbits of the planets are inclined by 3° to 8° to the Sun's equatorial plane (and the angle between the Sun's equatorial plane and the invariable plane of the solar system is 6.25°). These inclinations in conjunction with the solar oblateness give rise to torques on the Sun due to the planets. According to present knowledge, the oblateness of the Sun is essentially caused by rotational flattening of the outer layers, rather than by an internal quadrupole moment. Thus merely the convection zone, perhaps only its outer parts, will be directly affected by the planetary torques. One may expect, then, weak large-scale circulations to be induced or existing ones to be modulated, with an obvious potential to influence the activity cycle.

Though the interaction mechanisms discussed above are very weak, they may lead to significant effects if they act over a sufficiently long period of time. The relevant time-scale here is the age of the solar system ($4.5 \times 10^9$ years). The evolution of this system is characterized by an increasing synchronization of the orbital and rotational motions of its objects, caused by spin–orbit, orbit–orbit as well as more complicated couplings [38]. Where the coupling is so strong that the time-scale required to settle into a synchronized configuration is less than the age of the solar system, complete synchronization can be observed. Examples where this phenomenon was caused by spin–orbit coupling include the 1 : 1 synchronization of the orbital and rotational periods of the Earth's moon and of most other natural satellites and the 3 : 2 spin–orbit resonance of the planet Mercury. In other cases, where the coupling is weak, as for small satellites orbiting far from the parent planet (like the Saturnian satellite Hyperion), only partial synchronization seems to have been reached up to now. Similarly, the observed weak

synchronization of the SIM with the solar activity cycle may be a cumulative effect, resulting from the action of solar spin–orbit coupling, due for instance to the solar oblateness, over the last 4.5 billion years. Also, the solar oblateness may have been significantly larger during earlier phases of the solar evolution. An elaboration of these processes and their quantitative assessment are beyond the scope of this study.

## 7. Conclusion

Using the concept of synchronization analysis, we have quantitatively demonstrated that the solar activity cycle and the solar inertial motion are not independent. These two oscillatory phenomena are phase-synchronized during three epochs together accounting for almost half of the studied three-century observational data.

It is important that techniques of nonlinear data analysis have a potential to contribute to resolving long disputed problems such as the nature of the solar activity cycle. In an independent study, Paluš and Novotná [44] have recently observed nonlinear behavior of the sunspot cycle, namely its amplitude-frequency correlation. In this study we present quantitative evidence for a weak interaction of solar activity and gravity, i.e., for a weak influence of the movement of the giant planets of the solar system on the solar activity cycle. The existence of this weak interaction with still unknown physical mechanism does not mean that the SIM is the source of the solar cycle, neither is an argument against dynamo models. The phase synchronization is a phenomenon emerging in an interaction of two autonomous processes [19] which could evolve independently, or, due to a weak link, their phases could synchronize.

Recently, Winterhalder et al. [45] demonstrated that the synchronization analysis might not be specific regarding the dynamics of the underlying processes. This means that the presented analysis provides evidence for a dependence between the phases of the sunspot cycle and the SIM, but this does not automatically imply an explanation of the dependence by the physical mechanism of phase synchronization. The alternative hypothesis in [45], however, considers transfer function systems, in which one signal is obtained just as a filtration of the other, primary signal. We consider phase synchronization of two autonomous processes as the more plausible hypothesis for explaining the observed relation between the instantaneous phases of the sunspot cycle and the SIM. For further research and understanding of a possible coupling mechanism, it would be interesting to select a realistic dynamo model and propose a way how to simulate the interaction with the SIM. It is known from numerical studies of noisy oscillators and chaotic systems that even a very weak interaction can result in phase synchronized dynamics.

A special point here is to understand why the detected phase synchronization appears just in the observed intervals. In their previous studies, Charvátová [14,46,47] and Charvátová and Střeštík [13] identified the intervals 1730–1780 and 1910–1960 (almost coinciding with the above periods I and III) as recurring periods of ordered SIM (the SIM trajectories are ordered in a trefoil-like pattern). It is possible that the synchronized epochs recurred in the past and will recur in the future with the trefoil SIM periods which always occur after 178.7 years [13].

## Acknowledgements

This study was supported by the Grant Agency of the Academy of Sciences of the Czech Republic, projects No. IAA3042401 and A300120608, by the Institutional Research Plans AV0Z10300504 and AV0Z30420517; and by DFG SPP-1114 (*Mathematical Methods for Time Series Analysis and Digital Image Processing*).

## References

[1] K.L. Harvey (Ed.), The Solar Cycle, Astronomical Society of the Pacific Conference Series 27, San Francisco, 1992.
[2] F. Krause, K.-H. Rädler, Mean-Field Magnetohydrodynamics and Dynamo Theory, Pergamon Press, Oxford, 1980.
[3] M.R.E. Proctor, A.D. Gilbert (Eds.), Lectures on Solar and Planetary Dynamos, Cambridge Univ. Press, 1994.
[4] M. Ossendrijver, Astron. Astrophys. Rev. 11 (4) (2003) 287.
[5] U. Feudel, W. Jansen, J. Kurths, Int. J. Bif. Chaos 3 (1993) 131.
[6] M. Küker, R. Arlt, G. Rüdiger, Astron. Astrophys. 343 (1999) 977.
[7] N.O. Weiss, S.M. Tobias, Space Sci. Rev. 94 (2000) 99.
[8] M.D. Mundt, W.B. Maguire II, R.R.P. Chase, J. Geophys. Res. 96 (A2) (1991) 1705.
[9] M.N. Kremliovsky, Solar Phys. 151 (1994) 351.
[10] J. Kurths, H. Herzel, Physica D 25 (1987) 165.
[11] P.D. Jose, Astron. J. 70 (3) (1965) 193.
[12] R.W. Fairbridge, J.H. Shirley, Solar Phys. 110 (1987) 191.
[13] I. Charvátová, J. Střeštík, J. Atmos. Terrestrial Phys. 53 (11/12) (1991) 1019.
[14] I. Charvátová, Ann. Geophys. 18 (4) (2000) 399.
[15] M.G. Rosenblum, A.S. Pikovsky, J. Kurths, Phys. Rev. Lett. 76 (1996) 1804.
[16] M. Paluš, Phys. Lett. A 235 (1997) 341.
[17] C. Schäfer, M.G. Rosenblum, J. Kurths, H.H. Abel, Nature 392 (1998) 239.
[18] P. Tass, et al., Phys. Rev. Lett. 81 (1998) 3291.
[19] A. Pikovsky, M. Rosenblum, J. Kurths, Synchronization. A Universal Concept in Nonlinear Sciences, Cambridge Univ. Press, 2001.
[20] F. Cajori, Newton's Principia, Book III, Proposition XIII, University of California Press, San Francisco, 1934.
[21] M. Perryman, Rep. Progr. Phys. 63 (2000) 1209.
[22] J.H. Shirley, Programs for calculating the inertial motion of the Sun, J.H. Shirley, Jet Propulsion Laboratory, MS 183–601, Pasadena, CA 91109, USA, 1985. See, e.g., Ref. [12].
[23] T.C. Van Flandern, K.F. Pulkkinen, Astrophys. J. Suppl. 41 (1979) 391.
[24] G.M. Clemence, in: United States, Nautical Almanac Office, Astronomical papers prepared for the use of the American Ephemeris and Nautical Almanac 13, pt. 4, Washington, US Govt. Print. Off., 1953.
[25] X.X. Newhall, E.M. Standish, J.G. Williams, Astron. Astrophys. 125 (1983) 150.
[26] The sunspot series has been obtained from the SIDC-team, Royal Observatory of Belgium, Ringlaan 3, 1180 Brussels, Belgium. Internet address: http://sidc.oma.be/DATA/yearssn.dat.
[27] D. Gabor, J. IEE London 93 (1946) 429.
[28] R.L. Stratonovich, Topics in the Theory of Random Noise, Gordon and Breach, New York, 1963.
[29] J. Theiler, S. Eubank, A. Longtin, B. Galdrikian, J.D. Farmer, Physica D 58 (1992) 77.
[30] M. Paluš, Physica D 80 (1995) 186.
[31] J.A. Barnes, H.H. Sargent, P.V. Tryon, in: R.O. Pepin, J.A. Eddy, R.B. Merrill (Eds.), The Ancient Sun, Pergamon Press, New York, 1980, pp. 159–163.

[32] C. Allefeld, J. Kurths, Int. J. Bif. Chaos 14 (2) (2004) 406.
[33] M. Schüssler, P. Caligari, A. Ferriz-Mas, F. Moreno-Insertis, Astron. Astrophys. 281 (1994) L69.
[34] A. Ferriz-Mas, D. Schmitt, M. Schüssler, Astron. Astrophys. 289 (1994) 949.
[35] T. Landscheidt, Solar Phys. 189 (1999) 415.
[36] D.A. Juckett, Solar Phys. 191 (2000) 201.
[37] D. Juckett, Astron. Astrophys. 399 (2003) 731.
[38] C.D. Murray, S.F. Dermott, Solar System Dynamics, Cambridge Univ. Press, Cambridge, UK, 1999.
[39] E. Hantzsche, Astron. Nachr. 299 (1978) 259.
[40] V. Holzwarth, M. Schüssler, Astron. Astrophys. 405 (2003) 291.
[41] V. Holzwarth, M. Schüssler, Astron. Astrophys. 405 (2003) 303.
[42] M. Stix, The Sun. An Introduction, second ed., Springer, Berlin, 2002.
[43] S. Lorenzani, A. Tilgner, J. Fluid Mech. 492 (2003) 363.
[44] M. Paluš, D. Novotná, Phys. Rev. Lett. 83 (1999) 3406.
[45] M. Winterhalder, B. Schelter, J. Kurths, A. Schulze-Bonhage, J. Timmer, Phys. Lett. A 356 (2006) 26.
[46] I. Charvátová, Bull. Astron. Inst. Czechosl. 41 (1990) 200.
[47] I. Charvátová, Surv. Geophys. 18 (1997) 131.